Advances in Radiation Oncology (2021) 6, 100705

advances
in radiation oncology

www.advancesradonc.org

Scientific Article

Markerless Real-Time 3-Dimensional kV Tracking of Lung Tumors During Free Breathing Stereotactic Radiation Therapy

Kimmie de Bruin, MSc,[a] Max Dahele, PhD, MBChB, FRCR, FRCP,[a] Hassan Mostafavi, PhD,[b] Berend J. Slotman, MD, PhD,[a] and Wilko F.A.R. Verbakel, PhD, PDEng[a,*]

[a]*Department of Radiation Oncology, Amsterdam UMC, Vrije Universiteit Amsterdam, Cancer Center Amsterdam, Amsterdam, the Netherlands;* [b]*Varian Medical Systems, Palo Alto, California*

Received August 25, 2020; revised March 4, 2021; accepted March 30, 2021

Abstract

Purpose: Accurate verification of tumor position during irradiation could reduce the probability of target miss. We investigated whether a commercial gantry-mounted 2-dimensional (2D) kilo-voltage (kV) imaging system could be used for real-time 3D tumor tracking during volumetric modulated arc therapy (VMAT) lung stereotactic body radiation therapy (SBRT). Markerless tumor tracking on kV fluoroscopic images was validated using a life-like moving thorax phantom and subsequently performed on kV images continuously acquired before and during free-breathing VMAT lung SBRT.

Methods and Materials: The 3D-printed/molded phantom containing 3 lung tumors was moved in 3D in TrueBeam developer mode, using simulated regular/irregular breathing patterns. Planar kV images were acquired at 7 frames/s during 11 Gy/fraction 10 MV flattening filter free VMAT. 2D reference templates were created for each gantry angle using the planning 4D computed tomography inspiration phase. kV images and templates were matched using normalized cross correlation to determine 2D tumor position, and triangulation of 2D matched projections determined the third dimension. 3D target tracking performed on cone beam computed tomography projection data from 18 patients (20 tumors) and real-time online tracking data from 2 of the 18 patients who underwent free-breathing VMAT lung SBRT are presented.

Results: For target 1 and 2 of the phantom (upper lung and middle/medial lung, mean density −130 Hounsfield units), 3D results within 2 mm of the known position were present in 92% and 96% of the kV projections, respectively. For target 3 (inferior lung, mean density −478 Hounsfield units) this dropped to 80%. Benchmarking against the respiratory signal, 13/20 (65%) tumors (10.5 ± 11.1

Sources of support: This research was supported by a research grant from Varian Medical Systems.

Disclosures: The department has research collaborations with Varian Medical Systems. This work was sponsored by Varian and Dr Dahele, Dr Slotman, and Dr Verbakel have received honoraria/travel expenses from Varian Medical Systems. Dr Mostafavi has an issued patent US 9,008,398: Template matching method for image-based detection and tracking of irregular shaped targets, and an issued patent US 8,396,248: Sequential stereo imaging for estimating trajectory and monitoring target position, and he is an employee of Varian Medical Systems, Inc. Dr de Bruin reports grants and nonfinancial support from Varian Medical systems during the conduct of the study.

Research data are not available at this time, but sharing can be discussed upon request to the corresponding author.

Supplementary material for this article can be found at 10.1016/j.adro.2021.100705.

*Corresponding author: Wilko F.A.R. Verbakel, PhD, PDEng; E-mail: w.verbakel@amsterdamumc.nl

https://doi.org/10.1016/j.adro.2021.100705

cm^3) were considered successfully tracked on the cone beam computed tomography data. Tracking was less successful (≤50% of the time) in 7/20 (1.2 ± 1.5 cm^3). Successful online tracking during lung SBRT was demonstrated.

Conclusions: 3D markerless tumor tracking on a standard linear accelerator using template matching and triangulation of free-breathing kV fluoroscopic images was possible in 65% of small lung tumors. The smallest tumors were most challenging.

Introduction

Stereotactic body radiation therapy (SBRT) delivers high doses in a few fractions, with steep dose gradients. Five-year local control rates of ~90% have been reported for early stage peripherally located non-small cell lung cancer.[1] Many patients are treated during free-breathing. Respiration-induced tumor motion can be accounted for by using an internal target volume derived from a 4-dimensional (4D) computed tomography (CT) scan. However, a single 4DCT may underestimate lung tumor motion at the time of treatment.[2] Real-time tumor tracking during lung SBRT could therefore help to avoid a geographic miss by confirming that the target remains inside the planning target volume (PTV). It could also identify base-line tumor drift during delivery.[3] Although a direct link between geographic miss or underestimated motion and worse clinical outcomes has not been conclusively proven, there are some circumstantial data. For example, lower lobe tumor location has been linked to lower local control,[4] and tumors in the lower geometric quarter of the lung have been shown to be more mobile with more intrafraction motion variation.[5] This suggests a possible link between mobility, varying motion, and outcome, and supports positional verification that can identify when the tumor is outside the PTV, especially efforts that use relatively simple and inexpensive technology. External motion monitoring methods exist[6,7] but are surrogates for tumor motion. Markers implanted in the tumor can enable direct motion monitoring.[8] However, this is an invasive and costly procedure, not universally available, associated with medical risks, and markers can migrate.[9] Markerless monitoring of lung tumor position is desirable.

A gantry-mounted kilo-voltage (kV) imaging system is standard on many conventional linear accelerator (LINAC) platforms and some allow for continuous, fluoroscopic acquisition. Tracking using fluoroscopic kV images acquired during volumetric modulated arc therapy (VMAT) delivery has been successfully demonstrated for spine and breath-hold lung targets.[10-13] However, markerless 3D tracking of small lung tumors moving during breathing is challenging due to the motion, over-projection of internal structures, and low contrast with surrounding pixels. We investigated the feasibility of free-breathing markerless tracking using raw kV cone beam CT (CBCT) scan projections from lung SBRT patients. As the ground truth for clinical data are not known, the method was benchmarked using an anthropomorphic thorax phantom containing lung targets, moved in 3D by known amounts.

Methods and Materials

Markerless tracking

To determine 3D tumor position, nonclinical software for template generation, template matching, and triangulation (RapidTrack; Varian Medical systems) was used. This can be run online during image acquisition on a separate computer that is not connected to the treatment console or retrospectively offline on previously acquired images.

For every degree of gantry rotation, a 2D reference template (digitally reconstructed radiograph) was created comprising the delineated gross tumor volume (GTV) and a small margin using 1 phase of the planning 4DCT-scan (2.5 mm slice thickness; Discovery CT590 RT; GE Healthcare, Chicago, IL). Generating the templates, consisting of 360 images, takes ~2 minutes. The templates were prefiltered using a band-pass filter[9] (phantom data σlow = 0.4 mm/σhigh = 1.6 mm; patient data σlow = 0.6 mm/σhigh = 2.4 mm) to enhance structure edges and features and reduce (background) noise.

Planar kV images on the TrueBeam platform (Varian Medical Systems) can be acquired during CBCT acquisition (eg, full-fan [spot-light] CBCT at 15 frames per second [fps]) or by using kV fluoroscopy (3-15 fps) during VMAT treatment delivery. To determine the 2D position of the target on the projection images, they are automatically matched to the templates by calculating the normalized cross correlation within a patient-specific region of interest around the isocenter (ie, GTV plus its expected motion), resulting in a match score value between 0 and 1. A possible match is indicated by the highest peak in the match score surface; however, this might be an incorrect match (especially for noisy images with little contrast). For each match, a peak-to-sidelobe-ratio (PSR) is calculated. A minimum threshold for match score (MS) and PSR can be used to reject likely false matches.[14] Favorable settings for these thresholds were evaluated in the phantom study. The match results in a 2D position of the target for each image. To calculate the target's 3D coordinates, the

match results are triangulated[15] with 1 to 14 prior 2D matches over a separation angle of ≥20°.[16] Because the gantry speed is mostly in the range of 4°/s to 6°/s, the 3D tracking information was available after approximately 3 to 5 s. The prior 2D matches with a 3D distance between their tracking ray and the current image tracking ray (epipolar distance) <1.5 mm were selected for triangulation. If no tracking ray met this condition, the current match was rejected and not triangulated. In this way, the system is able to triangulate for moving targets.

Phantom study

To benchmark the accuracy of motion monitoring of lung tumors in free-breathing, a moving anthropomorphic thorax phantom was used.[17] The phantom is 3D printed/molded. It contains bony structures (3D printed in gypsum), airways and blood vessels ≥1 mm (printed in nylon), and soft tissue (silicone; cast in a 3D mold). There are 3 lung tumors (each ~4 cm^3; printed in nylon, Fig 1) located in the right upper lung, right middle lung (close to mediastinum), and left middle lung (with lower density, close to chest wall). Each tumor (GTV) was contoured (Eclipse; Varian Medical Systems) on a 3D planning CT-scan and a 4 mm isotropic margin was added for template generation.

During kV acquisition the phantom was either kept stationary or moved by programmed couch (table) motion in 3D using the TrueBeam Developer Mode (Varian Medical Systems). Regular and irregular breathing patterns were simulated to investigate the performance of the triangulation algorithm in an ideal situation (regular breathing) and a more realistic situation (irregular breathing). The regular breathing pattern had peak-to-peak amplitudes of 2/4.5/7.5 mm in lateral, longitudinal, and vertical directions, respectively. The irregular breathing pattern was simulated in the 3 directions with a direction-dependent multiplication factor combined with the equation: $y = 0.25 * \cos(2x) - 0.75 * \sin^2(1.1 * x) - \sin^3(x + 30) + (0.0003x) \wedge 2$, where x denotes a time-factor (72/s) and y the position. It had maximum peak-to-peak amplitudes of ~3.8/~9.5/~17.2 mm, respectively, and a phase and amplitude drift. Planar kV images were acquired with 100 kV tube voltage, 45 mA current, and 32 ms pulse width for a full arc at 7 fps during 5.5 Gy/arc 10 MV flattening filter free VMAT delivery.

The 2D and 3D root mean square error of measured versus known positions was calculated, and the percentage of matched frames with deviation <1, <2, and >5 mm from the expected location was determined. In addition, the influence of MS and PSR settings was evaluated. Both MS and PSR thresholds were set to zero for the remaining data.

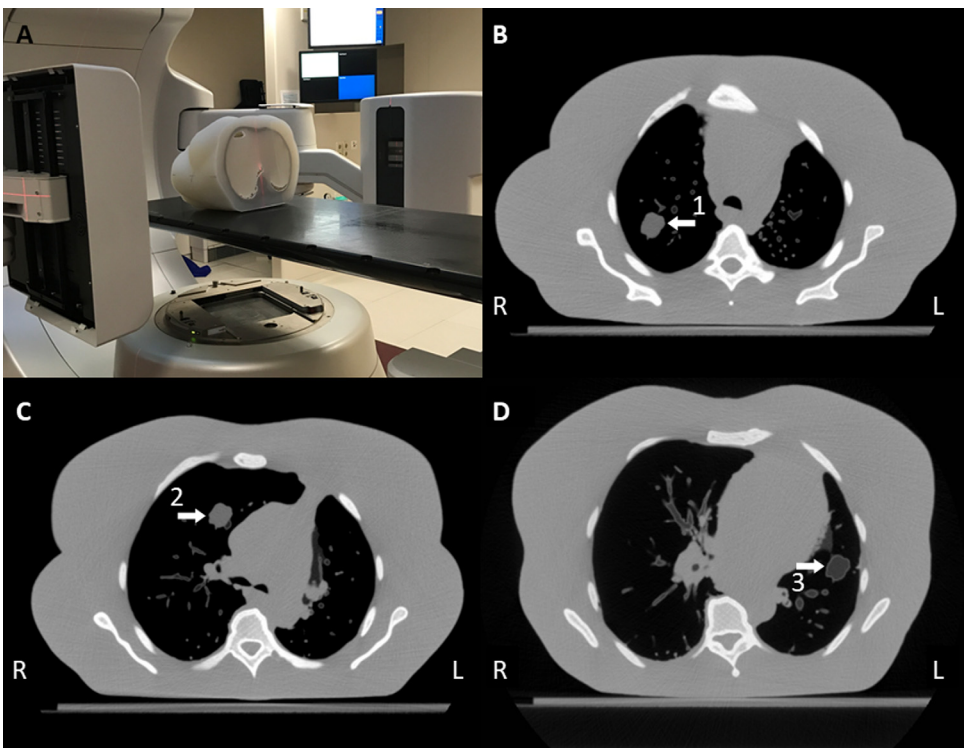

Figure 1 (A) Experimental setup for the phantom study. (B) Transverse slice of the (planning) computed tomography scan of the phantom at the level of target 1, (C) target 2, and (D) target 3. The arrows indicate the tumor in the right upper lung (1, mean Hounsfield unit [HU] = −130), the right middle lung (2, mean HU = −130), and the left middle lung (3, mean HU = −480).

Analysis of clinical data

A retrospective analysis was performed on 20 CBCT projection data sets from 18 serial patients undergoing free-breathing lung SBRT with various treatment schedules and tumor location/size/density/motion (Table 1). For the purposes of this analysis, the templates were generated from only 1 phase, the inspiration phase, of a 4D planning CT to minimize the effect of motion-related artefact and deformation of the tumor. The templates comprised the GTV plus a 4-mm isotropic margin (other margins can be used) to make available the tumor boundary and some surrounding tissues that move along with the tumor (eg, blood vessels) for the match. In some patients the template margin was empirically adjusted (eg, increased for very small tumors or decreased for large tumors, subtracting nearby structures, eg, rib or heart) to improve the tracking results (Table 1). For patient 17 the template was based on the expiration-phase GTV because the GTV was poorly visualized in inspiration.

Patients were positioned without rigid immobilization, typically with arms above the head. A full-fan 3DCBCT was acquired before the first treatment arc for target-based set-up and between the first and second arc to verify stability. Because the least deviation between actual target position and planned treatment position is expected in the CBCT between arcs, the raw data from these projections were used in the analysis, unless it had not been saved, in which case the first CBCT data set was used. The planar CBCT projections were acquired over an ~200° arc using 125 kV tube voltage, 30 mA current, and 20 ms pulse width at 15 fps. For each patient, 1 data set was analyzed. Positional deviations could originate from breathing motion, patient movement, matching error, and system inaccuracies. For patients 10 and 11, additional planar kV images were acquired with 125 and 100 kV tube voltage (respectively), 60 and 83 mA current, 25 and 15 ms pulse width, and 7 fps during a full arc 5.5 Gy/arc 10 MV flattening filter free VMAT delivery. The correlation between the vertical displacement of a 4-dot external Real-time Position Management (RPM) marker (Varian Medical Systems) and the longitudinal tumor trajectories (of both CBCT and during treatment)[18] was quantified by manually overlaying both graphs.

Results

Outlier rejection settings

Figure E1 shows a scatterplot of the PSR versus MS for different levels of error between the measured and actual positions of phantom targets 1, 2, and 3 under conditions of simulated irregular breathing motion. Although most matches with large deviation occurred for MS <0.35 and PSR <3.5, no optimal PSR and MS threshold could be determined without losing too many correct matches.

Phantom data

Table 2 summarizes the 2D and 3D tracking results for all breathing patterns of all 3 targets in the phantom, based on 422 to 428 projections. Figure 2 shows the motion trajectories for all 3 targets for the irregular breathing pattern over time and an example of the template, bandpass filtered kV projection and raw kV projection captured at gantry 0°.

Patient data

Figure 3 shows the measured motion trajectories for all patients. In the majority of the patients, a realistic motion trajectory with some outliers (pragmatically defined as large, unlikely spikes in the motion trajectory) was observed for the entire range of gantry angles (patients 1-12a; 13/20 [65%] trajectories, mean tumor volume 10.5 ± 11.1cm^3). Some targets moved little (patients 1-7a, mean cranio-caudal 4DCT motion 0.9 ± 1.1 mm) and some showed a clear motion profile consistent with a regular breathing pattern (patients 7b-12a, mean cranio-caudal 4DCT motion 9.5 ± 2.9 mm). Although we have no ground-truth data for the position of the tumor, the trajectories corresponded with the motion of the external RPM marker on the chest, and we considered these as "successfully" tracked. In other cases, tracking was less successful, with more outliers and no or only partially realistic motion profiles (patients 12b-18; 7/20 [35%] trajectories, mean tumor volume 1.2 ± 1.5 cm^3). For some of those patients, tracking was still possible for up to approximately half of the time (patients 15-17), whereas for other gantry angles tracking was less successful; nonetheless, we have included all of these patients in the group that was "less-successfully" tracked.

For the patients with successful tracking (patients 1-12a), the estimated displacement from the motion trajectory was compared with the target displacement identified by the CBCT match. This was within 2 mm in 92%, 75%, and 92% of the cases for the lateral, longitudinal, and vertical directions, respectively. The peak-peak amplitude of these trajectories (patients 1-12a, except for patient 10) was compared with the peak-peak amplitude of the (planning) 4DCT and corresponded within 2 mm in 92%, 62%, and 85% of the cases for the lateral, longitudinal,

Table 1 Clinical data (revised)

Patient	SBRT schedule	GTV volume (cm^3)	Template margin	Peak-peak amplitude dX (mm)	Peak-peak amplitude dY (mm)	Peak-peak amplitude dZ (mm)	Peak-peak amplitude 3D (mm)	Initial set-up CBCT (S) or between arcs (A)	Mean HU* (ROI inside GTV center plane)
1	5 × 11 Gy	1.4	4 mm - rib	3	0	3	4	A	−32
2	5 × 11 Gy	1.4	4 mm	0	2	0	2	S	−263
3	8 × 7.5 Gy	40.6	0 mm	0	0	0	0	S	−667
4	5 × 11 Gy	21.1	1 mm	6	2	4	7	A	−138
5	5 × 11 Gy	5.6	4 mm - rib	2	0	2	3	S	−133
6	5 × 11 Gy	2.1	4 mm	2	2	4	5	A	123
7a	8 × 7.5 Gy	14.6	1 mm	0	0	0	0	S	−130
7b	5 × 11 Gy	10.4	1 mm	1	12	1	12	S	−270
8	5 × 11 Gy	18.3	1 mm	0	10	4	11	A	25
9	8 × 7.5 Gy	5.3	5 mm	0	10	4	11	A	−24
10	5 × 11 Gy	4.4	2 mm	1	10	4	11	A	−67
11	5 × 11 Gy	7.3	4 mm - rib	0	9	6	11	A	15
12a	5 × 11 Gy	1.0	8 mm	0	12	2	12	A	26
12b	5 × 11 Gy	0.6	4 mm	0	0	0	0	A	−202
13	8 × 7.5 Gy	0.4	4 mm	0	4	2	4	S	−147
14	11 × 5 Gy	1.2	4 mm	1	10	4	15	S	−200
15	3 × 18 Gy	0.6	8 mm	2	8	0	8	A	−398
16	5 × 11 Gy	7.8	4 mm	0	4	1	4	S	−314
17	8 × 7.5 Gy	0.8	5 mm - heart GTV50%	4	5	0	6	A	−97
18	3 × 18 Gy	0.1	8 mm	3	3	2	5	S	−178

Abbreviations: 3D = 3-dimensional; CBCT = cone beam computed tomography; CT = computed tomography; GTV = gross tumor volume; HU = Housenfeld units; ROI = region of interest; SBRT = stereotactic lung radiation therapy.

* The estimated density should be treated with caution because it was derived using a 2D ROI in the axial center plane on the planning CT of the GTV in inspiration phase. The reader should also consult the corresponding images in Figure 3 to obtain a realistic overview of the tumor characteristics.

Table 2 Tracking results phantom data

	Breathing pattern	2D RMS error (mm)	3D RMS error (mm)	3D matched frames after triangulation (%)*	3D matched frames with error <1 mm (%)†	3D matched frames with error <2 mm (%)†	Outliers 2D, error >3 mm (%)‡	Outliers 3D, error >3 mm (%)‡
Target 1	Stationary	1.9	3.6	93.1	86.0	92.1	6.1	5.8
	Regular	2.2	4.4	89.1	79.5	90.4	8.8	5.2
	Irregular	2.2	3.0	88.3	82.5	92.9	9.0	5.1
Target 2	Stationary	1.5	1.4	94.1	84.7	94.7	5.7	2.9
	Regular	1.6	1.3	90.3	86.9	96.9	5.3	2.2
	Irregular	1.7	1.6	89.7	85.2	95.8	5.5	2.9
Target 3	Stationary	3.1	4.7	93.8	67.7	81.6	18.1	14.5
	Regular	4.1	4.8	87.2	68.2	79.6	22.3	17.1
	Irregular	4.0	4.7	89.0	65.9	78.7	22.4	16.2

Abbreviations: 2D = 2-dimensional; RMS = root mean square.

* The percentage of 3D matched frames left after rejection according to epipolar distance during the triangulation process (see text).

† The percentage of 3D matched frames (after template matching + triangulation and after rejection during triangulation) for which the error between measured and known position was <1 or 2 mm.

‡ The percentage of outliers in the 2D and 3D data, defined as error between measured and known position >3 mm.

and vertical direction, respectively. Patient 10 was excluded because the longitudinal motion trajectory was very irregular, but its tracking amplitude ranged up to 20 mm in longitudinal direction, whereas this was only 10 mm on the 4DCT. Another 4DCT of this patient showed again a much larger amplitude, confirming a substantial variation in breathing depth.

Figure 4 shows the measured motion trajectories versus the RPM signal (both longitudinal direction) of CBCT data and data during MV delivery of patient 10 and 11. For patient 10 some distortion is visible in the final part of the tracking trace during MV delivery, caused by saturation of the imager by too high mAs.

Discussion

Near real-time 3D markerless free breathing lung tumor tracking using 2D kV projections was feasible in the majority of patients, and the accuracy of the methodology, benchmarked on a highly anthropomorphic thorax phantom, was within 2 mm in 80% to 96% of matched frames, depending on the characteristics of the simulated target (lowest for the least dense tumor in the phantom). The triangulation algorithm appeared to perform equally well during regular and irregular breathing motion. We were unable to find matching parameter thresholds that would enable automatic, selective rejection of all (potential) outliers.

The 3 targets in the phantom showed variation in the tracking accuracy (Table 2). All 3 tumors had the same size and volume, but target 3 had the lowest density (−480 mean Hounsfield units),[17] resulting in little contrast on many of the kV images and the worst tracking performance (errors in tracked position and tracking outliers). Tumor location (and therefore also overlying projections and image acquisition angle) can also affect tumor visibility.[11,19] The tracking accuracy of target 1 cranial in the right lung might have been affected by the projection of dense overlying structures in the shoulder area. When tracking during VMAT irradiation, the image acquisition angle depends on the treatment arc. Although certain arc directions may increase tumor visibility on the fluoroscopy images,[20] these directions may not be optimal for achieving ideal treatment planning dose distributions.

Although the patient data are qualitative, despite an inability to benchmark the tracked tumor position against its (unknown) true position or to see the tumor in the images, clear breathing-related motion patterns can be observed and outliers can be visually distinguished. Indeed, comparing the measured trajectories with the scaled-up RPM signal (Fig 4) shows a similar pattern with an identical breathing phase, supporting our methodology. On average, the trackable patients had a larger tumor volume and were denser. The percentage of

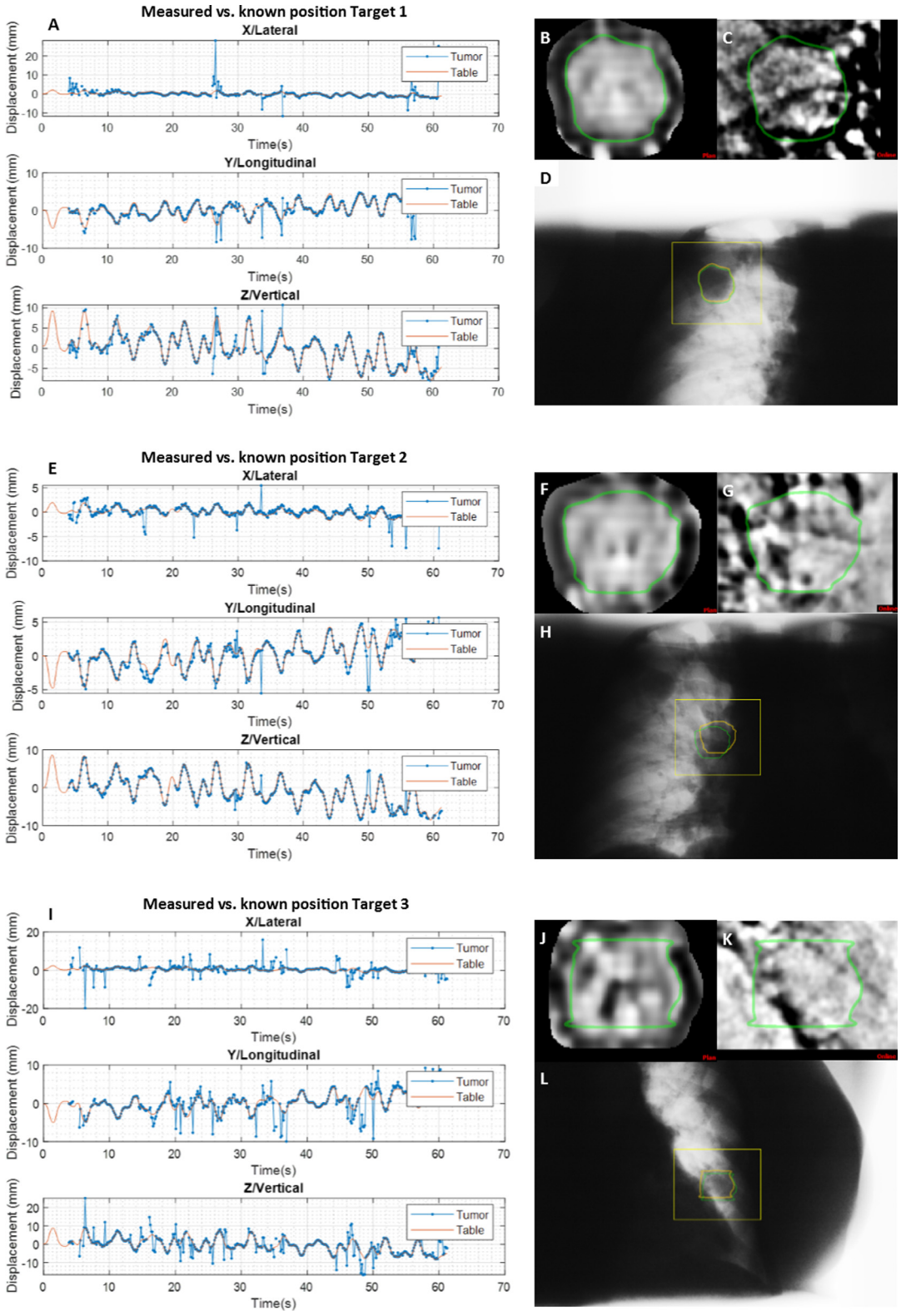

Figure 2 Motion trajectories of target 1 A, target 2 E, and target 3 I, showing the measured (blue, tumor) and known (orange, table) positions. (B, F, and J) The bandpass filtered template, (C, G, and K) the cropped bandpass filtered kilo-voltage projection, (D, H, and L) and the unfiltered kilo-voltage projection at gantry 0˚ of target 1, 2, and 3. Where at t = 0 seconds, 15 seconds, 30 seconds, 45 seconds, and 60 seconds, the gantry is at ~180˚, 90˚, 0˚, 270˚, and 180˚, respectively.

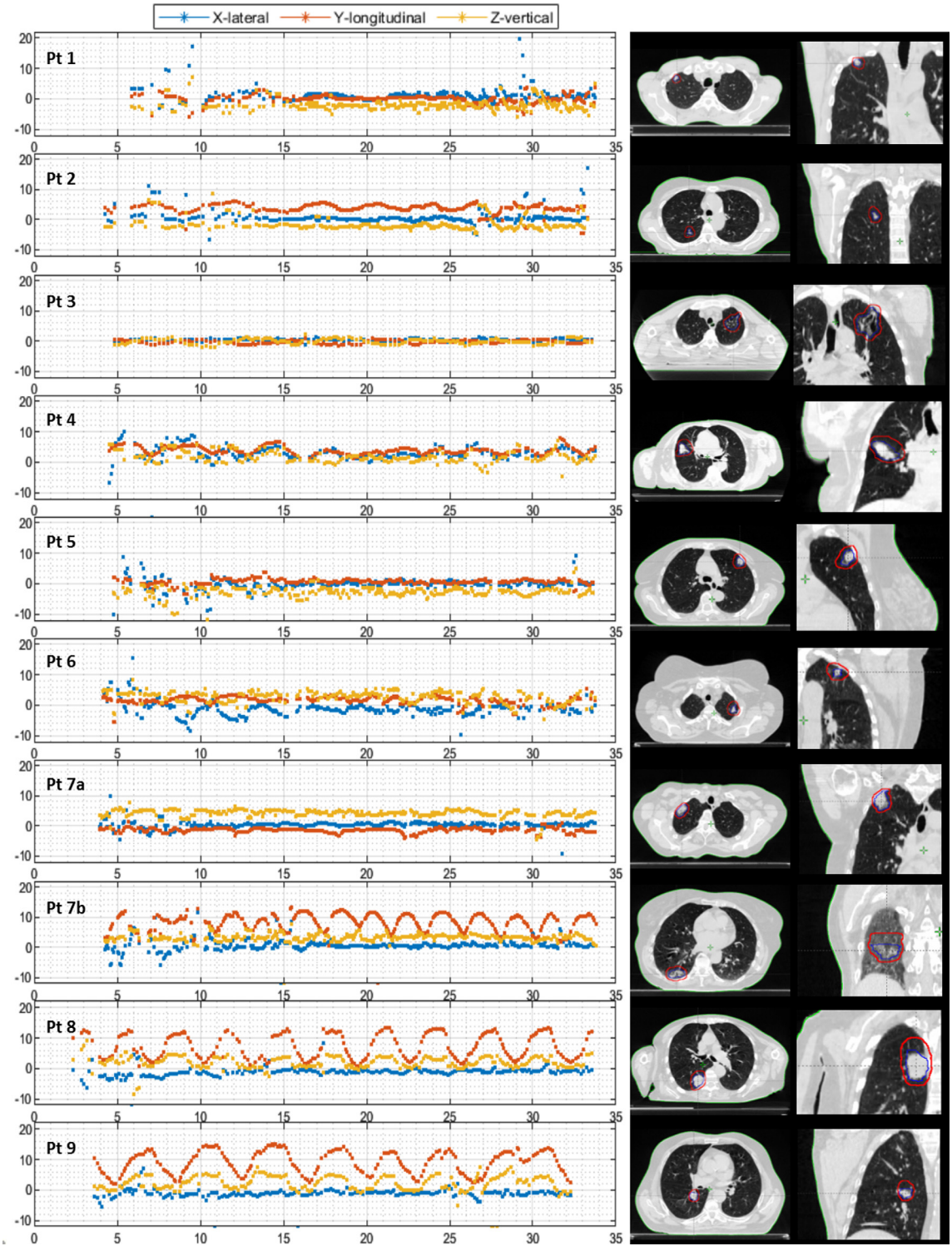

Figure 3 (A) Left: The motion trajectories of patient 1-9 in 3 directions: lateral (blue), longitudinal (red), and vertical (yellow). Right: Transverse slice of the (planning) computed tomography scan at inspiration phase of the corresponding patient at the level of the tumor (blue contour = gross tumor volume, red contour = planning target volume). (B) Left: The motion trajectories of patient 11-18 in 3 directions: lateral (blue), longitudinal (red), and vertical (yellow). Right: Transverse slice of the (planning) computed tomography scan at inspiration phase of the corresponding patient at the level of the tumor (blue contour = gross tumor volume, red contour = planning target volume).

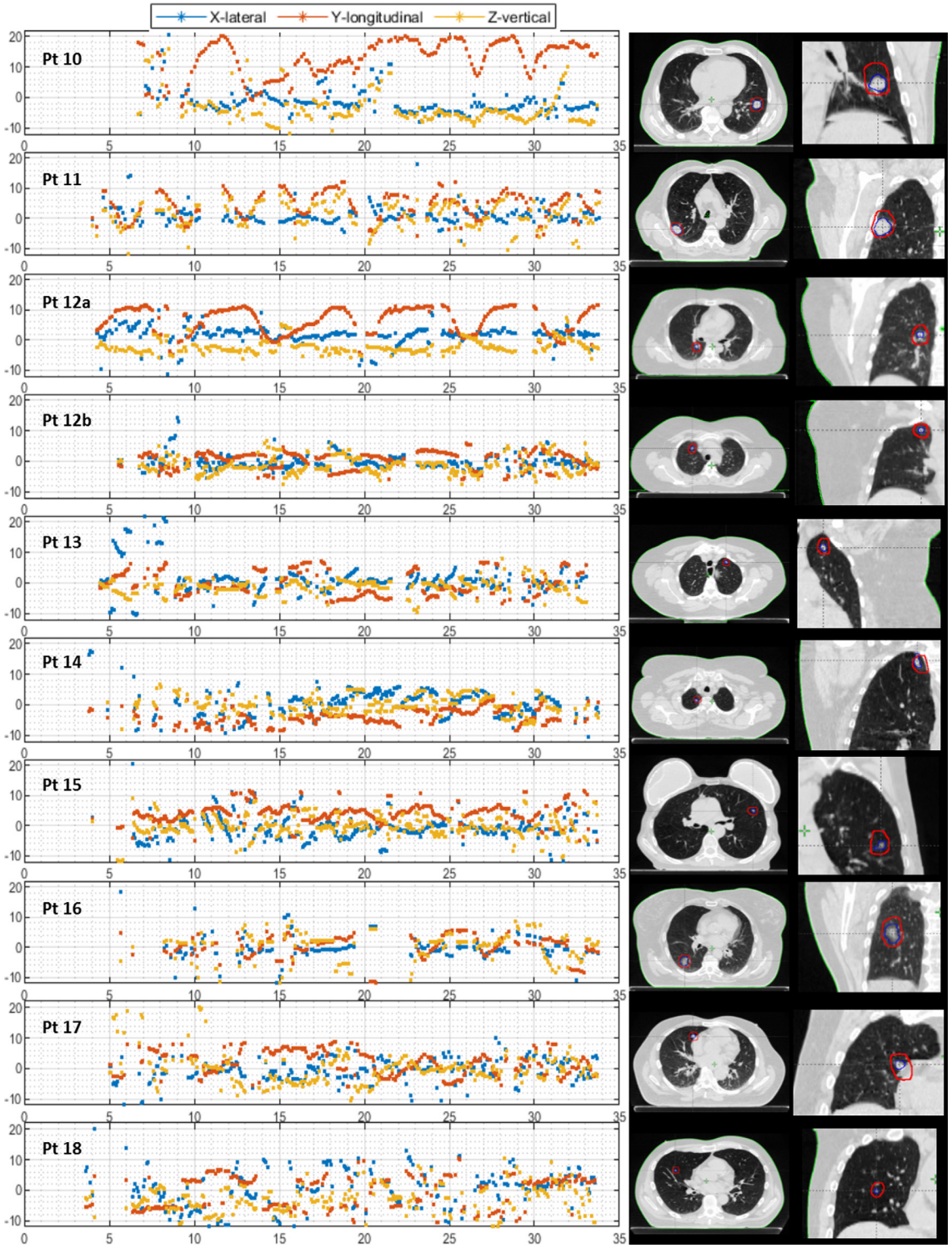

Figure 3 **Continued.**

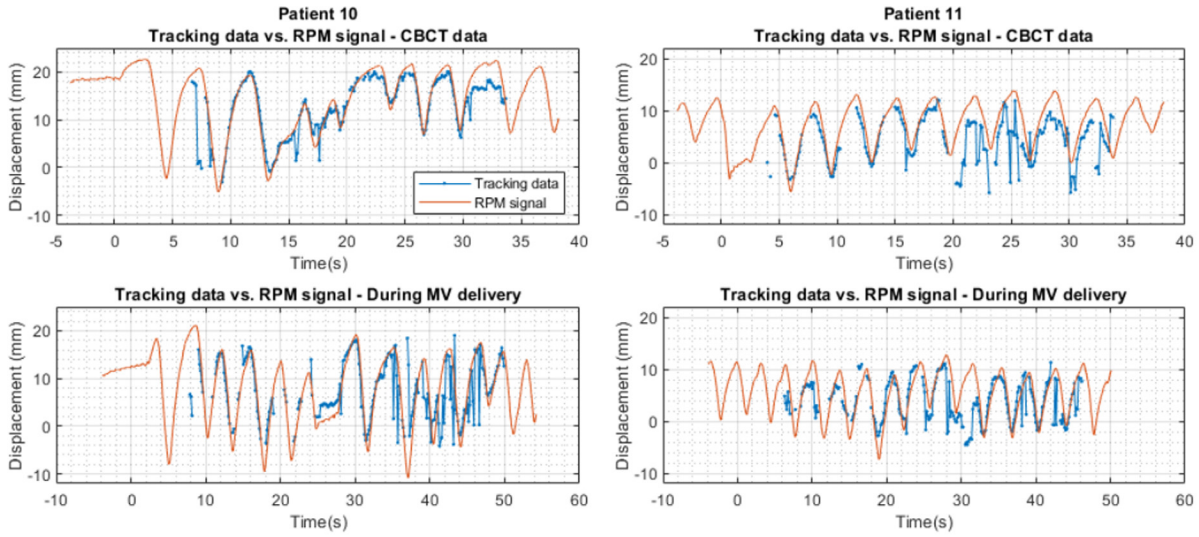

Figure 4 The measured motion trajectories (blue) versus the Real-time Position Management signal (orange) in longitudinal direction of cone beam computed tomography data and data during MV delivery of patients 10 and 11. The Real-time Position Management signal has been scaled for each patient with a fixed (patient-specific) factor to match the tracking data. *Abbreviations:* CBCT = cone beam computed tomography; RPM = Real-time Position Management.

trackable patients compares favorably with work by Bahig et al[19] using the CyberKnife fiducial-less XSight-Lung tracking system based on orthogonal radiographs. Although they tracked 66% of targets, these tumors were preselected based on favorable characteristics, including larger size (all >1.5 cm), density, and peripheral location. In the current data set (which did not include tumors in an extreme caudal location), the influence of tumor location was difficult to determine. We did observe that in certain cases difficulty in tracking was encountered at particular gantry angles, for example when the tumor was located close to the heart.

Earlier work demonstrated limitations of triangulation of near-stationary targets.[11] A (gradual) displacement in the vertical and/or lateral direction caused errors in the 3D position, because the triangulation is performed on sequential images separated in time. Here, we use triangulation for, in many cases, periodically but irregularly moving targets. When the tracking method described here was used for tracking irregular spine motion, a high-contrast structure in the phantom facilitating template matching, 99.2% of the measured 3D spine positions were within 1 mm of the expected location (3D root mean square error 0.5 mm).[13] From this we conclude that the triangulation algorithm can perform under conditions of irregular motion, but challenges arise in template-matching low-contrast images.

Lower tumor density, overlying structures, and (poor/reduced) image quality decrease (lung) tumor visibility on the 2D kV projections, and therefore make template matching challenging. Small size may also make tracking harder.[19] It is notable that even when tracking is generally poor, not all gantry angles lead to incorrect matches. Sometimes, a few kV images are matched well, alternating with images with a large match error. The current system matches every image individually without taking into account information from previous matches, which could improve template matching capabilities. Accepting too many false matches can lead to larger 3D errors due to triangulation of erroneous 2D positions. Matches are rejected in the triangulation process when the threshold of the epipolar distance between the prior and current tracking rays is exceeded, and a decrease in the amount and percentage of outliers is observed (Table 2). However, this does not result in the rejection of all incorrect matches. Therefore, additional methods (MS and PSR threshold) were tested, but these were suboptimal for the task of selectively rejecting incorrect matches. However, we have previously shown the benefits of digital tomosynthesis (DTS) for motion monitoring of low-contrast lung tumors in breath-hold. By using multiple previous images, DTS increases the visibility of the target while blurring over-projecting structures, allowing accurate monitoring of stationary tumors under steady breath-hold conditions.[11] Due to the respiratory motion of targets in our study, DTS is not appropriate as it can only identify the tumor position averaged over the DTS angle.[21] Possible ways of improving the matching merit investigation, including automatic rejection of false matches, improved image quality, multiple template matches, and deep-learning based techniques.[22-24] With respect to dose from the kV tracking procedure, this is in the range of that from a CBCT.[13] To reduce cumulative dose the CBCT between arcs could be omitted if tracking is reliable, or the CBCT can be reconstructed from the fluoroscopic data obtained during the arc.[25]

By monitoring the position of moving lung tumors during irradiation, the chance of PTV underdosing due to geographic miss[2] might be reduced. It could also facilitate verification of gated delivery and eventually allow for more individualized target volumes and PTV margins. Other studies have used stereoscopic kV images and were able to track in 3D with sub-mm accuracy under simplified phantom conditions,[26,27] but the method described here compares very favorably. Zhang et al[28] proposed a markerless tracking system based on simultaneously acquired MV/kV imaging. Although this overcomes the ~3 s start of tracking delay in our method with a triangulation separation angle of 20°, more information about clinical performance is needed, for example, lung tumor visualization might be challenging due to high energy photons and shielding by the multi-leaf collimator. Integrated magnetic resonance imaging has recently become clinically available, and some clinics provide real-time tracking and gating of lung tumors treated with SBRT.[29] However, this is not widely available, it is expensive, and at the moment only single-plane 2D tracking is available based on deformable image registration, with uncertain accuracy under clinical conditions. Furthermore, our own departmental experience with magnetic resonance image-based lung tumor tracking[29] is that failure to track small lung tumors is not uncommon, in which case such patients are transferred to the conventional LINAC for treatment.

In conclusion, 3D markerless tumor tracking based on template matching and triangulation of free-breathing kV fluoroscopic images acquired on a standard commercial LINAC was possible in the majority of small lung tumors. Further improvements will enable next-generation conventional LINAC-based image guided radiotherapy.

Supplementary materials

Supplementary material associated with this article can be found in the online version at https://doi.org/10.1016/j.adro.2021.100705.

References

1. Senthi S, Lagerwaard FJ, Haasbeek CJ, et al. Patterns of disease recurrence after stereotactic ablative radiotherapy for early stage non-small-cell lung cancer: A retrospective analysis. *Lancet Oncol*. 2012;13:802–809.
2. Steiner E, Shieh CC, Caillet V, et al. Both four-dimensional computed tomography and four-dimensional cone beam computed tomography under-predict lung target motion during radiotherapy. *Radiother Oncol*. 2019;135:65–73.
3. Shaverdian N, Veruttipong D, Wang J, et al. Location, location, location: Lower lobe stage I non-small cell lung cancer treated with stereotactic body radiation therapy are associated with poor outcomes. *Int J Radiat Oncol Biol Phys*. 2016;96:E427.
4. Knybel L, Cvek J, Molenda L, et al. Analysis of lung tumor motion in a large sample: patterns and factors influencing precise delineation of internal target volume. *Int J Radiat Oncol Biol Phys*. 2016;96:751–758.
5. Peguret N, Dahele M, Cuijpers JP, et al. Frameless high dose rate stereotactic lung radiotherapy: Intrafraction tumor position and delivery time. *Radiother Oncol*. 2013;107:419–422.
6. Bertholet J, Knopf A, Eiben B, et al. Real-time intrafraction motion monitoring in external beam radiotherapy. *Phys Med Biol*. 2019;64:15TR01.
7. Caillet V, Booth JT, Keall P. IGRT and motion management during lung SBRT delivery. *Physica Medica*. 2017;44:113–122.
8. Shimizu S, Shirato H, Ogura S, et al. Detection of lung tumor movement in real-time tumor-tracking radiotherapy. *Int J Radiat Oncol Biol Phys*. 2001;51:304–310.
9. Imura M, Yamazaki K, Shirato H, et al. Insertion and fixation of fiducial markers for setup and tracking of lung tumors in radiotherapy. *Int J Radiat Oncol Biol Phys*. 2005;63:1442–1447.
10. Hazelaar C, Verbakel WF, Mostafavi H, et al. First experience with markerless online 3D spine position monitoring during SBRT delivery using a conventional LINAC. *Int J Radiat Oncol Biol Phys*. 2018;101:1253–1258.
11. Hazelaar C, Dahele M, Mostafavi H, et al. Markerless positional verification using template matching and triangulation of kV images acquired during irradiation for lung tumors treated in breath-hold. *Phys Med Biol*. 2018;63:115005.
12. van Sörnsen de Koste JR, Dahele M, Mostafavi H, et al. Markerless tracking of small lung tumors for stereotactic radiotherapy. *Med Phys*. 2015;42:1640–1652.
13. Hazelaar C, Dahele M, Mostafavi H, et al. Subsecond and submillimeter resolution positional verification for stereotactic irradiation of spinal lesions. *Int J Radiat Onc Biol Phys*. 2016;94:1154–1162.
14. Mostafavi H, Sloutsky A, Jeung A. Detection and localization of radiotherapy targets by template matching. *Ann Int Conf IEEE Eng Med Biol Soc*. 2012:6023–6027.
15. Mostafavi H, Sloutsky A, inventors; Varian Medical Systems Inc, assignee. Sequential stereo imaging for estimating trajectory and monitoring target position. United States patent US 8,396,248. 2013 Mar 12.
16. Hazelaar C, van der Weide L, Mostafavi H, et al. Feasibility of markerless 3D position monitoring of the central airways using kilovoltage projection images: managing the risks of central lung stereotactic radiotherapy. *Radiother Oncol*. 2018;129:234–241.
17. Hazelaar C, van Eijnatten M, Dahele M, et al. Using 3D printing techniques to create an anthropomorphic thorax phantom for medical imaging purposes. *Med Phys*. 2018;45:92–100.
18. Fayad H, Pan T, Clement JF, Visvikis D. Technical note: Correlation of respiratory motion between external patient surface and internal anatomical landmarks. *Med Phys*. 2011;38:3157–3164.
19. Bahig H, Campeau MP, Vu T, et al. Predictive parameters of CyberKnife fiducial-less (XSight Lung) applicability for treatment of early non-small cell lung cancer: A single-center experience. *Int J Radiat Oncol Biol Phys*. 2013;87:583–589.
20. Furtado H, Seppenwoolde Y, Steiner E, et al. OC-0210: Motion management for partial arc VMAT treatments using intra-fractional 2D/3D registration. *Radiother Oncol*. 2016;119:S95–S96.
21. van Sörnsen de Koste JR, Dahele M, Mostafavi H, et al. Digital tomosynthesis (DTS) for verification of target position in early stage lung cancer patients. *Med Phys*. 2013;40. 091904.
22. Parsons D, Robar JL. An investigation of kV CBCT image quality and dose reduction for volume-of-interest imaging using dynamic collimation. *Med Phys*. 2015;42:5258–5269.
23. Haytmyradov M, Mostafavi H, Wang A, et al. Markerless tumor tracking using fast-kV switching dual-energy fluoroscopy on a benchtop system. *Med Phys*. 2019;46:3235–3244.

24. Teske H, Mercea P, Schwarz M, et al. Real-time markerless lung tumor tracking in fluoroscopic video: Handling overlapping of projected structures. *Med Phys*. 2015;42:2540–2549.
25. Hazelaar C, Dahele M, Scheib S, Slotman BJ, Verbakel WFAR. Verifying tumor position during stereotactic body radiation therapy delivery using (limited-arc) cone beam computed tomography imaging. *Radiother Oncol*. 2017;123:355–362.
26. Jung J, Song SY, Yoon SM, et al. Verification of accuracy of CyberKnife tumor-tracking radiation therapy using patient-specific lung phantoms. *Int J Radiat Oncol Biol Phys*. 2015;92:745–753.
27. Ziegler M, Lettmaier S, Fietkau R, et al. Performance of makerless tracking for gimbaled dynamic tumor tracking. *Zeitschrift für Medizinische Physik*. 2020;30:96–103.
28. Zhang P, Hunt M, Telles AB, et al. Design and validation of a MV/kV imaging-based markerless tracking system for assessing real-time lung tumor motion. *Med Phys*. 2018;45:5555–5563.
29. Finazzi T, Palacios MA, Haasbeek CJ, et al. Stereotactic MR-guided adaptive radiation therapy for peripheral lung tumors. *Radiother Oncol*. 2020;144:46–52.